Mapping 24 woody plant species phenology and ground forests phenology over China from 1951-2020

Mengyao Zhu[1], Junhu Dai[1,2,3], Huanjiong Wang[1], Juha M. Alatalo[4], Wei Liu[1,2], Yulong Hao[1,2], Quansheng Ge[1,2]

[1]Key Laboratory of Land Surface Pattern and Simulation, Institute of Geographic Sciences and Natural Resources Research, Chinese Academy of Sciences, Beijing, 100101, China
[2]College of Resources and Environment, University of Chinese Academy of Sciences, Beijing, 101408, China
[3]China-Pakistan Joint Research Center on Earth Sciences, CAS-HEC, Islamabad, 45320, Pakistan
[4]Environmental Science Centre, Qatar University, Doha, 2713, Qatar

Correspondence to: Junhu Dai (daijh@igsnrr.ac.cn); Quansheng Ge (geqs@igsnrr.ac.cn)

Abstract. Plant phenology refers to the cyclic plant growth events, and is one of the most important indicators of climate change. Integration of plant phenology information is crucial for understanding ecosystem response to global change and modeling the material and energy balance of terrestrial ecosystems. Utilizing 24,552 in-situ phenological observations of 24 representative woody plants species from the Chinese Phenology Observation Network (CPON), we have developed maps delineating species phenology (SP) and ground phenology (GP) of forests over China from 1951-2020. These maps offer a detailed spatial resolution of 0.1° and a temporal resolution of 1day. Our method involves a model-based approach to upscale in-situ phenological observations to SP maps, followed by the application of weighted average and quantile methods to derive GP maps from the SP data. The resulting SP maps for the 24 woody plants exhibit a high degree of concordance with in-situ observations, manifesting an average deviation of 6.9 days for spring and 10.8 days for autumn phenological events. Moreover, the GP maps demonstrate robust alignment with extant Land Surface Phenology (LSP) products sourced from remote sensing data, particularly within deciduous forests, where the average discrepancy is 8.8 days in spring and 15.1 days in autumn. This dataset provides an independent and reliable phenology data source for China on a long-time scale of 70 years, and contributes to more comprehensive research on plant phenology and climate change at both regional and national scales. The dataset can be accessed at https://doi.org/10.57760/sciencedb.07995 (Zhu et al., 2023).

1 Introduction

Plant phenology, the discipline that examines the timing of plant life cycle events, emerges in response to the seasonal changes in climate and environmental conditions (Lieth, 1974; Schwartz, 2003). These events are pivotal stages in a plant's life, such as budburst, leaf unfolding, flowering, leaf coloring, and defoliation. Recognized as a sensitive biological indicator of climate change (Fu et al., 2015; Richardson et al., 2013), plant phenology is instrumental in understanding ecosystem responses to global change (Menzel et al., 2020) and is a significant factor in modeling the exchanges of matter and energy within terrestrial ecosystems (Keenan et al., 2014). The demand for extensive, long-term, and reliable plant phenology data

is pronounced among researchers for effective biological monitoring and predictive studies. Although such data are now available from various sources (Piao et al., 2019; Tang et al., 2016), including in-situ observations (Templ et al., 2018), satellite remote sensing (Bolton et al., 2020; Dixon et al., 2021), and tower-based digital cameras (Richardson et al., 2018), harmonizing this information across broad spatial and temporal scales remains a significant scientific challenge, complicated by inconsistencies among data sources (Fisher et al., 2006; Park et al., 2021).

The practice of conducting manual, in-situ observations for species phenology (SP) boasts a rich history extending over several centuries (Aono and Kazui, 2008), yielding highly accurate data for specific plant species (Polgar and Primack, 2011). In 1963, the Chinese Academy of Sciences established the Chinese Phenology Observation Network (CPON), which stands as a benchmark for phenological data collection through its standardized, nationwide network, engaging numerous professional observers and an extensive repository of ground-based observations. CPON's repository, to date, encompasses over 1.2 million records for upwards of 900 plant species from more than 150 sites across China (Fig. 1), cementing its dominant status as a data center for phenological research in China. These phenology records have been contributed to examining the spatio-temporal patterns of plant phenological shifts (Dai et al., 2014; Ge et al., 2015), the environmental factors affecting plant phenology (Dai et al., 2013; Wang et al., 2020), and the development of phenology models in China (Tao et al., 2018). However, the spatial distribution of in-situ data is often uneven and limited, particularly at regional and global scales (Donnelly et al., 2022), with significant gaps over extended timescales. Advances in species-level phenology modeling offer a promising avenue to overcome these spatial and temporal constraints (Fu et al., 2020; Hufkens et al., 2018). In scenarios lacking of direct phenological observations, such models are invaluable for generating large-scale predictions, thereby filling in the missing data gaps in both space and time (Cleland et al., 2007; Wang et al., 2012). This modeling approach has been exemplified by the Extended Spring Indices (SI-x) model, which has produced detailed gridded maps delineating the first leaf and first bloom events for three woody plants across the contiguous United States with resolutions from 1° to 1 km (Ault et al., 2015; Izquierdo-Verdiguier et al., 2018). Adopting a similar strategy, it is feasible to extrapolate the CPON phenology observations across China, facilitating the integration and scaling up of this rich dataset to serve regional and national research needs.

In contrast to manual in-situ observations, satellite remote sensing facilitates expansive monitoring and mapping of land surface phenology (LSP) at a landscape scale, yielding more comprehensive phenological data (Studer et al., 2007). Over the past four decades, remote sensing technologies have witnessed substantial enhancements, leading to significant strides in both spatial and temporal resolution (Misra et al., 2020; Dronova and Taddeo, 2022). Currently, a variety of LSP products, based on vegetation indices like NDVI and EVI from diverse remote sensing sources, provide LSP data on regional and global scales with resolutions from 10 km down to 30 m (e.g., Li et al., 2019; Wu et al., 2021). The reliability of these LSP datasets is highly dependent on validation against ground phenology (GP) data derived from in-situ SP observations (Tian et al., 2021; Zhang et al., 2017), necessitating a seamless transition from individual (i.e., SP) to landscape (i.e., GP) level. Methods such as weighted averages and quantiles have proven their efficacy in this aggregation process from individual to community or landscape levels (Donnelly et al., 2022; Fitchett et al., 2015). For instance, the weighted average method has

been validated at the site scale through combined field and remote sensing studies to aggregate GP data from in-situ SP observations, considering species abundance as weights (Liang et al., 2011). Recent studies have suggested that quantile methods (e.g., 30th percentile) holds greater promise than the commonly used average methods at larger scales, as demonstrated in Europe and the USA (Ye et al., 2022). Nevertheless, such methods have not yet been applied to aggregate large-scale GP from SP data in China. This gap potentially limits the ground-truthing for LSP products and hampers a comprehensive understanding of the spatial and temporal patterns of phenological shifts over the country.

In this study, we aimed to develop long-term, high-resolution SP and GP maps of China, spanning from 1951 to 2020 with a 0.1° resolution. This effort will produce spatially continuous, gridded phenology products that are notably missing in the current Chinese context, yet are vital for diverse scientific and ecological applications. Drawing from the extensive database of the CPON, we analyzed 24,552 in-situ phenology observations of 24 representative woody plants from 122 sites over six decades. This analysis included three critical phenophases for each species: the first leaf date (FLD), first flower date (FFD), and 100% leaf coloring date (LCD). In our methodology, we employed five species-level phenology models with gridded meteorological data to simulate SP maps. To refine these maps for each plant species, we applied species distribution maps as spatial filters. We further synthesized these SP maps into GP maps, utilizing weighted average and quantile methods that incorporated the distribution probabilities of the species as weights. The SP maps underwent a rigorous cross-validation process to ensure accuracy, while the GP maps' reliability was verified through comparative analysis with existing LSP products. The contribution of this study is the introduction of a novel grid phenology dataset for China. This dataset enhances the spectrum of available phenology data within the country and serves as an independent source for validating LSP products. Moreover, it is expected to significantly advance research on plant phenology and global change by providing a more detailed portrayal of the spatiotemporal trends in plant phenology patterns.

2 Methods

2.1 Data acquisition and processing

2.1.1 Phenology observations

The in-situ phenology observations from 1963 to 2018 were obtained from the CPON. We selected 24 representative woody plants species across 17 families (Table 1). These species are not only prevalent in China’s forest ecosystems (Fang et al., 2011), but also extensively recorded within CPON database. The longitudinal span of these observations covers 55 years across 122 sites, with a total of 24,552 individual records, covering a diverse spectrum of land cover, ecological, and climatic conditions across China (Fig. 1). Each species in the study has a substantial representation in the dataset, with at least 40 years of phenologucal data from a minimum of 13 distinct sites. We focused on three phenophases for each species: spring FLD, spring FFD, and autumn LCD. To ensure the integrity of the dataset, we applied three-sigma limits, a statistical filter that retains data within three standard deviations from the species' mean phenological dates (Pukelsheim, 1994).

Outliers that fell beyond these thresholds were excluded, as they constitute less than 1% of the data points on a standard normal distribution, ensuring a robust and reliable dataset for analysis.

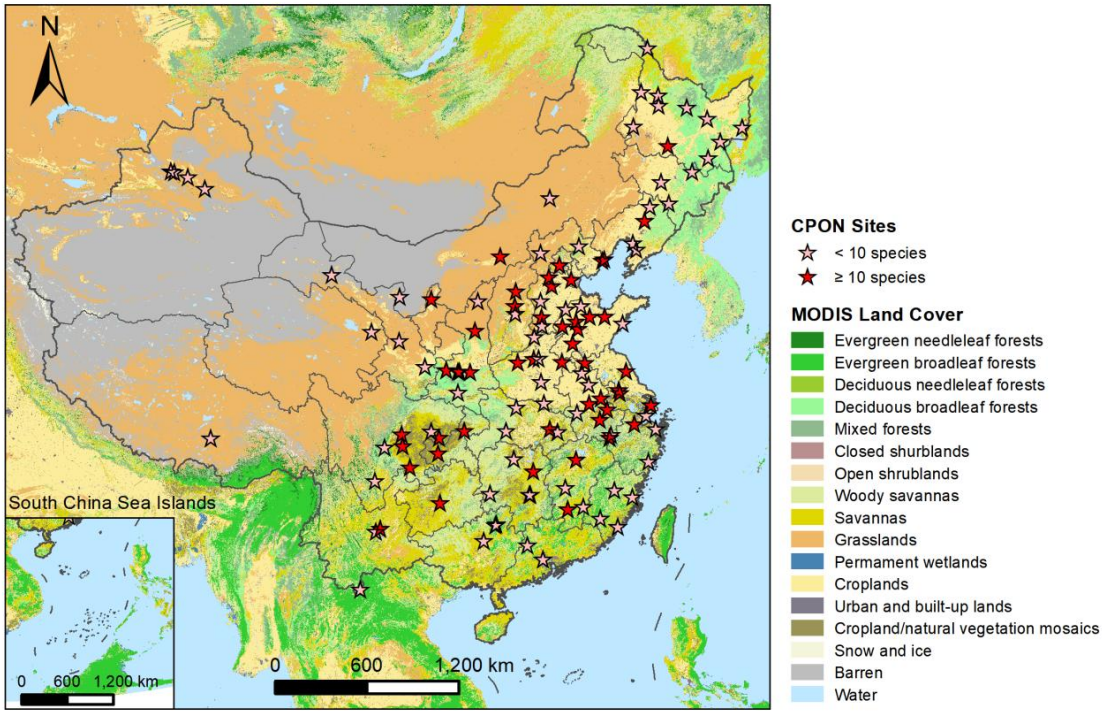

Figure 1: Geographic distribution of CPON sites (n = 122) included in the phenology dataset across China. Sites with less than 10 recorded species are marked with pink asterisks, while sites with more than 10 recorded species are marked with red asterisks. Note that the markings on the map of several adjacent sites may overlap each other. The background map shows the IGBP land cover type from the MODIS Land Cover product (Friedl and Sulla-Menashe, 2022).

Table 1: List of 24 species of woody plants from 17 families in China. Number of records represents the total number of three phenophases (FLD, FFD and LCD) of all sites and all years for each species.

No.	Species	Family	Life form	Number of sites	Number of years	Number of records
1	*Ginkgo biloba*	Ginkgoaceae	Tree	45	49	1110
2	*Metasequoia glyptostroboides*	Cupressaceae	Tree	37	47	860
3	*Magnolia denudata*	Magnoliaceae	Tree	42	47	980
4	*Salix babylonica*	Salicaceae	Tree	65	42	1526

5	*Populus × canadensis*	Salicaceae	Tree	43	51	954
6	*Robinia pseudoacacia*	Fabaceae	Tree	54	45	1757
7	*Albizia julibrissin*	Fabaceae	Tree	36	47	984
8	*Cercis chinensis*	Fabaceae	Shrub	52	49	1207
9	*Prunus armeniaca*	Rosaceae	Tree	46	45	950
10	*Ulmus pumila*	Ulmaceae	Tree	60	44	1428
11	*Morus alba*	Moraceae	Tree	50	50	1071
12	*Broussonetia papyrifera*	Moraceae	Tree	41	43	1103
13	*Quercus acutissima*	Fagaceae	Tree	17	40	292
14	*Pterocarya stenoptera*	Juglandaceae	Tree	29	46	936
15	*Juglans regia*	Juglandaceae	Tree	50	47	816
16	*Betula platyphylla*	Betulaceae	Tree	13	43	369
17	*Acer pictum* subsp. *mono*	Sapindaceae	Tree	18	46	492
18	*Ailanthus altissima*	Simaroubaceae	Tree	34	47	873
19	*Melia azedarach*	Meliaceae	Tree	61	46	1410
20	*Firmiana simplex*	Malvaceae	Tree	57	48	1403
21	*Hibiscus syriacus*	Malvaceae	Shrub	58	47	1096
22	*Fraxinus chinensis*	Oleaceae	Tree	23	40	505
23	*Syringa oblata*	Oleaceae	Shrub	50	51	1163
24	*Paulownia fortunei*	Paulowniaceae	Tree	49	48	1267
Total		-	-	122	55	24552

2.1.2 Climate data

The daily mean temperature (T) data spanning from 1950 to 2020 were sourced from two distinct repositories: (1) Site-specific temperature (Site T) was retrieved from the China Meteorological Data Service Center (CMDSC, https://data.cma.cn/). This dataset was primarily utilized for parameterizing the phenology models. (2) Gridded temperature (Grid T) was derived from the ERA5-Land climate reanalysis datasets (Muñoz Sabater, 2019; Muñoz-Sabater et al., 2021), available through the Copernicus Climate Change Service (C3S, https://cds.climate.copernicus.eu/). Grid T was employed for phenology simulation and upscaling processes, with a fine spatial resolution of 0.1°, approximately equating to 10 km.

To obtain daily grid T values, we computed the average from hourly temperature data recorded at four distinct times of the day (4:00, 10:00, 16:00, 22:00).

The current bioclimatic variables (BIOCLIM+) were obtained from Climatologies at High Resolution for the Earth Land Surface Areas (CHELSA, https://chelsa-climate.org/) to determine the species distribution (Brun et al., 2022a, b). These variables encapsulate the average ecological and climatic conditions for the period 1981-2010, boasting a high resolution of 0.0083°. From the available bioclimatic data, we extracted both the traditional set of 19 bioclimatic layers (Bio1-Bio19) and an additional set of 50 layers. To mitigate the effects of autocorrelation among these bioclimatic variables, we computed the correlation coefficient between each pair of layer. Variables exhibiting a correlation coefficient above 0.8 relative to preceding layers were omitted to prevent redundancy. Consequently, a subset of 12 bioclimatic layers was selected for inclusion as the environmental variables within the species distribution models (detailed in Table S1). These selected layers were then resampled to a 0.1° resolution to ensure consistency with the resolution of the grid T data.

2.1.3 Forest and species distribution data

The forest distribution map of China was sourced from the dataset of "Annual Dynamics of Global Land Cover and its Long-term Changes from 1982 to 2015" dataset (Liu et al., 2020). To discern forested regions, we reclassified the annual land cover (LC) layers into 'forest' and 'non-forest' categories. We then determined the duration of forest cover by summing the annual layers, and pixels representing at least one year of forest cover were identified as forest distribution areas. For forest type categorization, we employed the widely recognized International Geosphere-Biosphere Program (IGBP) classification system from the MODIS Land Cover Type (MCD12C1) Version 6.1 data product (Friedl and Sulla-Menashe, 2022). In our classification scheme, we combined evergreen needleleaf forest (class 1) and evergreen broadleaf forest (class 2) to delineate evergreen forest category. Similarly, deciduous needleleaf (class 3) and deciduous broadleaf forest (class 4) were amalgamated into deciduous forest category. The mixed forest (class 5) category was retained as is.. To achieve a consistent spatial resolution across our datasets, both the forest distribution map and forest type map were resampled from their original 0.05° resolutio to a 0.1° resolutio using the majority method, to match the resolution of the grid T data.

The county-level species distribution maps were sourced from the comprehensive Database of China's Woody Plants (Fang et al., 2011). This authoritative database consolidates distribution data from an exhaustive suite of national, provincial, and regional floristic surveys and inventory reports published in China up to 2009 (Cai et al., 2021). Additionally, we obtained 4,371 occurrence records for 24 selected woody plant species from the Global Biodiversity Information Facility (GBIF, 2022; https://www.gbif.org/), which were subsequently utilized as the occurrence data inputs for species distribution modeling (detailed in Table S2). To ensure the reliability of our data, we included only those occurrence records that had location coordinate with an uncertainty of less than 2,000 meters. Moreover, the dataset was meticulously cleansed to eliminate any duplicate records, thereby enhancing the robustness of the species distribution models employed in our analysis.

2.2 Generating species phenology maps using a model-based upscaling method

The generation of SP maps involves two major processes: (1) generating species potential phenology maps, and (2) generating species distribution maps. The definitive SP maps emerged from the spatial intersection of these two distinct map types, effectively overlaying the potential phenology with the actual distribution to pinpoint precise phenological patterns.. The workflow for the processes is shown in Fig. 2.

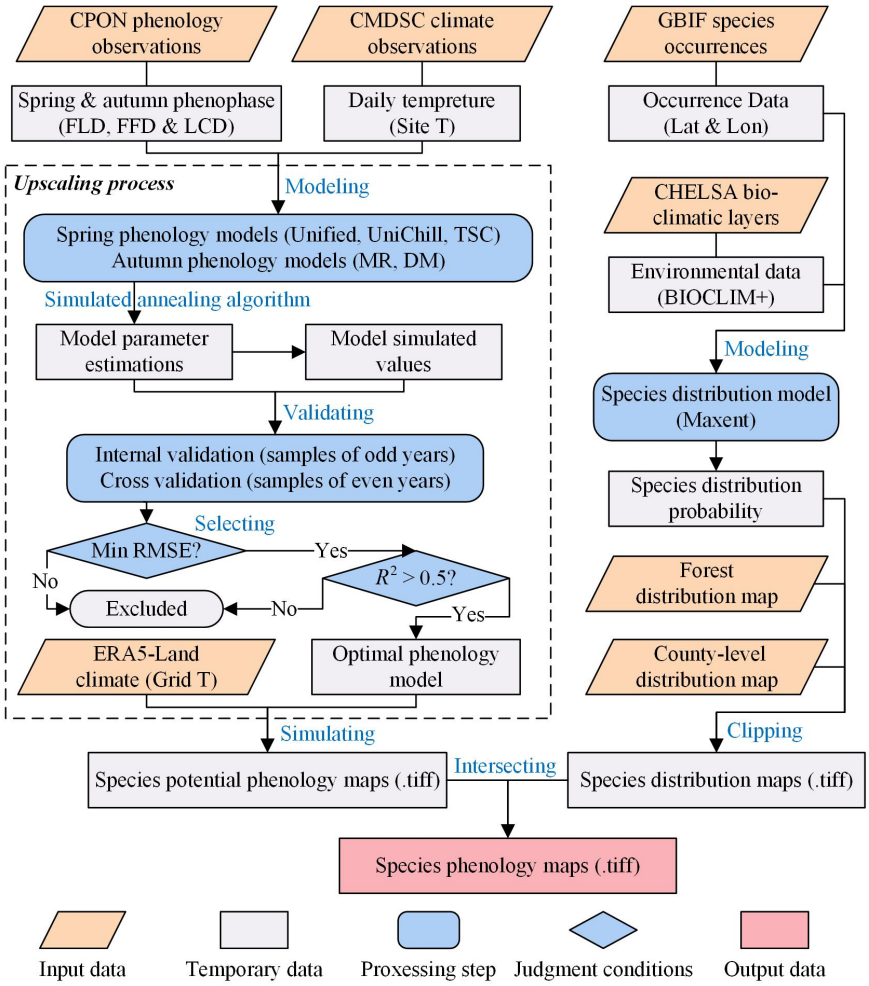

Figure 2: The workflow of generating SP maps using a model-based upscaling method, which involves two major processes: (1) Generating species potential phenology maps, and (2) Generating species distribution maps. The words in blue color represent the key processes of data generation. ".tiff" indicates the GeoTIFF format of the grid phenology or distribution maps.

2.2.1 Species potential phenology maps

In the first process, we employed a model-based upscaling method to transform in-situ phenology observations into gridded phenology maps. Phenology models were constructed utilizing the phenophases (i.e., FLD, FFD, LCD) recorded by the CPON, in conjunction with the site T from the CMDSC climate observations. For each species under study, we developed a suite of phenology models to the respective seasonal phases. Three models were designated for spring phenology: the Unichill, Unified (Chuine, 2000) and temporal-spatial coupling (TSC) models (Ge et al., 2014). And two models were designated for autumn phenology: the multiple regression (MR) (Estrella and Menzel, 2006) and temperature-photoperiod (TP) models (Delpierre et al., 2009). The details of the modeling formulae and their respective parameters are elaborated upon in Appendix S1. The modeling strategy involved a cross-validation approach, where data from odd years were used for model training, while data from even years were set aside for model validation purposes. The estimation of all model parameters was executed via the simulated annealing algorithm (Chuine et al., 1998), ensuring a robust optimization process for the phenology models.

For model validation, the models' root mean square error (RMSE) and goodness of fit (R^2) were calculated between the model predicted values and the original observed values. We conducted an internal validation using the data from odd years to evaluate the models' fitting efficacy. On the other hand, we conducted a cross validation was ondata from even years to evaluate the models' capability to simulate and extrapolate phenology data beyond the sample used for model development. The optimal phenology model for each species was determined as the one with the smallest RMSE during the cross-validation process and an R^2 exceeding 0.5 (or 0.3 for LCD) during both validation processes. Species for which no model met these predefined criteria were omitted from the subsequent generation of SP and GP maps.

To simulate SP maps, we input daily grid T data from ERA5-Land climate reanalysis into the previously determined optimal phenology models for each species. The simulation was conducted on a pixel-by-pixel basis, enabling the interpolation and upscaling of phenology observations from discrete sites to a comprehensive gridded phenology maps (Chuine et al., 2000). It is important to note, however, that the availability of grid T data allows for the simulation of species phenology, even in areas lacking observed species distribution. Therefore, we refer to the resultant maps as species potential phenology maps. This distinction emphasizes that while the simulated values represent potential phenological events based on climatic variables, they should not be misconstrued as actual observed values in regions where the species does not exist.

2.1.2 Species distribution maps

In the second process, species distribution maps were generated by integrating species distribution models with county-level species distribution data. For each species, we constructed models using the Maximum Entropy Species Distribution Modelling (Maxent; Phillips et al., 2006) version.3.4.4. Maxent is a widely utilized tool in species distribution modeling due to its efficacy in estimating a species' distributional range by finding the distribution pattern with maximum entropy (i.e., closest to the uniform). Maxent models the likelihood of species presence across geographical grids, assigning a predicted

probability of occurrence to each grid cell. To configure the Maxent model, we utilized occurrence data from the GBIF database, paired with environmental data inputs from the 12 bioclimatic layers provided by BIOCLIM+. In the model parameter settings, both linear and quadratic feature types were used to capture the relationship between species presence and environmental variables. Additionally, to validate the model and assess its predictive performance, we employed a 5-fold cross validation method.

To evaluate the accuracy of the Maxent species distribution models, we applied the receiver operating characteristic (ROC) curve analysis. The integral of the ROC curve, referred to as the area under the curve (AUC), serves as a quantitative measure of the model's prediction accuracy (Fielding and Bell, 1997). An AUC value approaching 1.0 is indicative of a model with high predictive accuracy. In our study, the Maxent models demonstrated robust predictive power, with an average test AUC of 0.845 and a standard deviation of 0.043 across the different species (Table S2).

2.3 Generating ground phenology maps using weighted average and weighted quantile methods

In our study, we aggregated individual-level SP maps into landscape-level GP maps using four aggregation methods: (1) weighted average (mean); (2) weighted median (pct50); (3) weighted 20th percentile (pct20) for spring phenology or weighted 80th percentile (pct80) for autumn phenology; (4) weighted 10th percentile (pct10) for spring phenology or weighted 90th percentile (pct90) for autumn phenology. Previous studies typically utilized species abundance as weights for aggregation at a local scale, but obtaining such data at the regional scale proves challenging. Therefore, we replaced species abundance with species distribution probability as aggregation weight for each species. This assumption stems from the positive correlation between species distribution and abundance (Brown, 1984), indicating that species tend to exhibit higher abundance in the core of their geographic range (Sagarin and Gaines, 2002). The aggregation techniques applied in this study (e.g., pct50, pct20\80 and pct10\90) are analogous to the methods used for extracting LSP from remote sensing data (e.g., midpoint, dynamic threshold and maximum curvature). The procedures followed in the generation of GP maps are illustrated in Fig. 3.

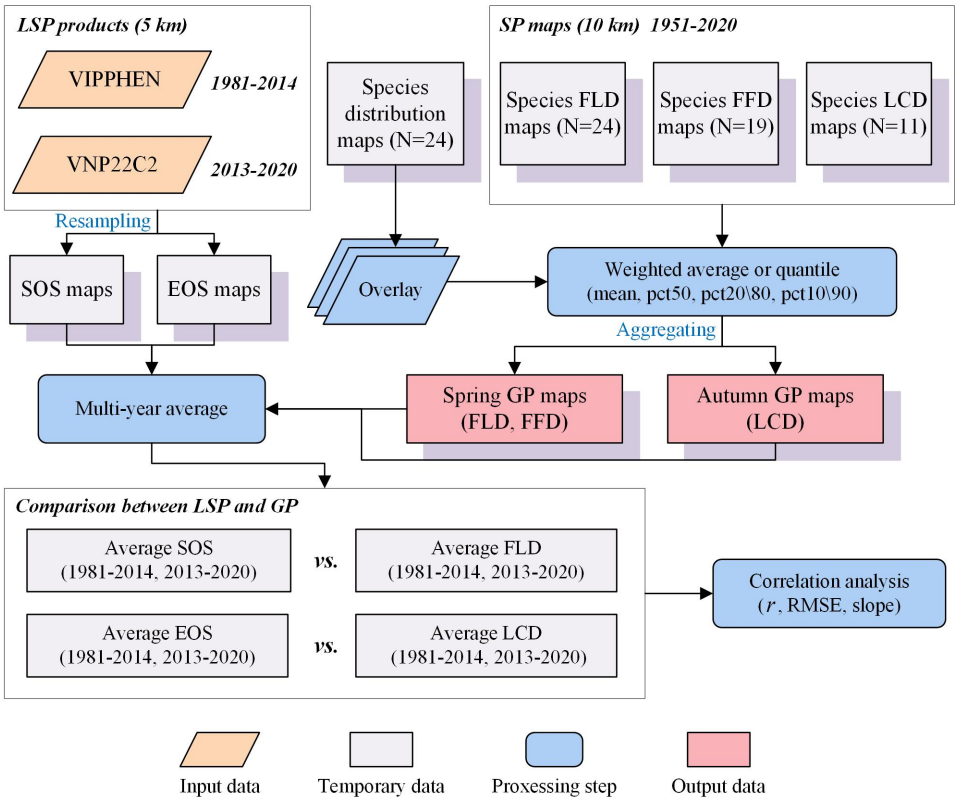

Figure 3: The workflow of generating GP maps from SP maps, and comparing GP maps with two LSP products. The words in blue color represent the key processes of data generation.

For n species, the phenological data were first arranged in ascending order. The SP of each species is y_i ($i = 1, 2, \ldots, n$), and the distribution probability of each species is p_i ($i = 1, 2, \ldots, n$). Then, the aggregated GP (Y_{mean} and $Y_{pct}(x\%)$) was calculated according to the following formulas:

$$\omega_i = \frac{p_i}{\sum_{i=1}^{n} p_i} \quad (1)$$

$$W_j = \sum_{i=1}^{j} \omega_i, j = 1,2,\ldots,n \quad (2)$$

$$Y_{mean} = \sum_{i=1}^{n} \omega_i \times y_i \quad (3)$$

$$Y_{pct} = \begin{cases} y_1, if\ W_1 > x \\ (y_j - y_{j-1}) \times \frac{x - W_{j-1}}{\omega_j}, if\ W_j > x, W_{j-1} < x \\ y_n, if\ W_{n-1} < x \end{cases} \quad (4)$$

where ω_i is a weight to each species, W_j is the cumulative weight from the 1st to the j-th species, $x\%$ is the percentile tag which takes values from 10%, 20%, 50%, 80% and 90%. These calculations enable the construction of aggregated GP maps by combining species phenology maps with species distribution maps and weighting them by species distribution probability.

To evaluate the data quality and reliability of the aggregated GP maps, we undertook a comparative analysis with two established LSP products derived from remote sensing data: (1) VIPPHEN_NDVI dataset (1981-2014), utilized the midpoint method to extract the start of season (SOS) and the end of season (EOS) from the AVHRR data (Didan and Barreto, 2016); (2) VNP22C2 datasetproduct (2013-2020), utilized the maximum curvature method to derive SOS and EOS from the MODIS data (Zhang et al., 2020). To align the spatial resolution of these datasets with our GP maps, we resampled both LSP products from 5 km to 0.1° using the average method. Subsequently, we conducted a correlation analysis to assess the consistency between our GP data and the LSP products, specifically comparing the FLD with SOS for the spring, and the LCD with EOS for the autumn. The comparison involved averaging the LSP and GP maps across two distinct periods: 1981-2014 and 2013-2020. The statistical measures calculated for this assessment included the Pearson correlation coefficient (*r*), RMSE, and linear regression slope between GP and LSP across different forest types (Table S3).

3 Results and discussion

The dataset encompasses two distinct types of phenology maps over China: (1) Annual SP maps for 24 woody plants species, constructed using the model-based upscaling method; (2) Annual GP maps for forest vegetation, generated by four aggregation methods, accompanied by quality assurance (QA) maps. These maps detail the phenological events of FLD, FFD in spring, and LCD in autumn, spanning from 1951 to 2020, with a spatial resolution of 0.1° and a temporal resolution of 1 day. Each phenology map is stored as a 16-bit signed integer within GeoTIFF file format, comprising a two-dimension raster (641 row × 361 column). The phenology data are expressed in Julian Day of the year (DOY), indicating the elapsed number of days from January 1st to the occurrence of phenological event. The dataset's valid DOY values range from 1 to 366, while null values are denoted by -1.

3.1 Simulation and validation of species phenology maps

The SP maps of FLD (24 species), FFD (19 species), and LCD (12 species) were generated by applying the optimal phenology models. Here, we present the results of the SP maps for four emblematic woody species (Fig. 4), including ginkgo (*Ginkgo biloba*), willow (*Salix babylonica*), elm (*Ulmus pumila*), and lilac (*Syringa oblata*). These maps have been refined using species distribution maps to ensure that the simulated phenologies were relevant only to areas where the species are known to exist. The presented maps illustrate a clear spatial pattern in the timing of phenophases correlated with latitude. Specifically, the onset of spring event such as FLD and FFD for these species is markedly delayed with increasing latitude. Conversely, the autumn LCD occurs earlier as the latitude increases. While these spatial patterns are consistent across

species, there are notable temporal differences at the same latitudes, For example, at lower latitudes, the elm exhibits an earlier FFD in spring and a later LCD in autumn compared to the other species. Phenophases for some species were not included in the simulation, because the suboptimal explanatory power of their phenology models, e.g., $R^2 < 0.5$ for spring FFD, and $R^2 < 0.3$ for autumn LCD.

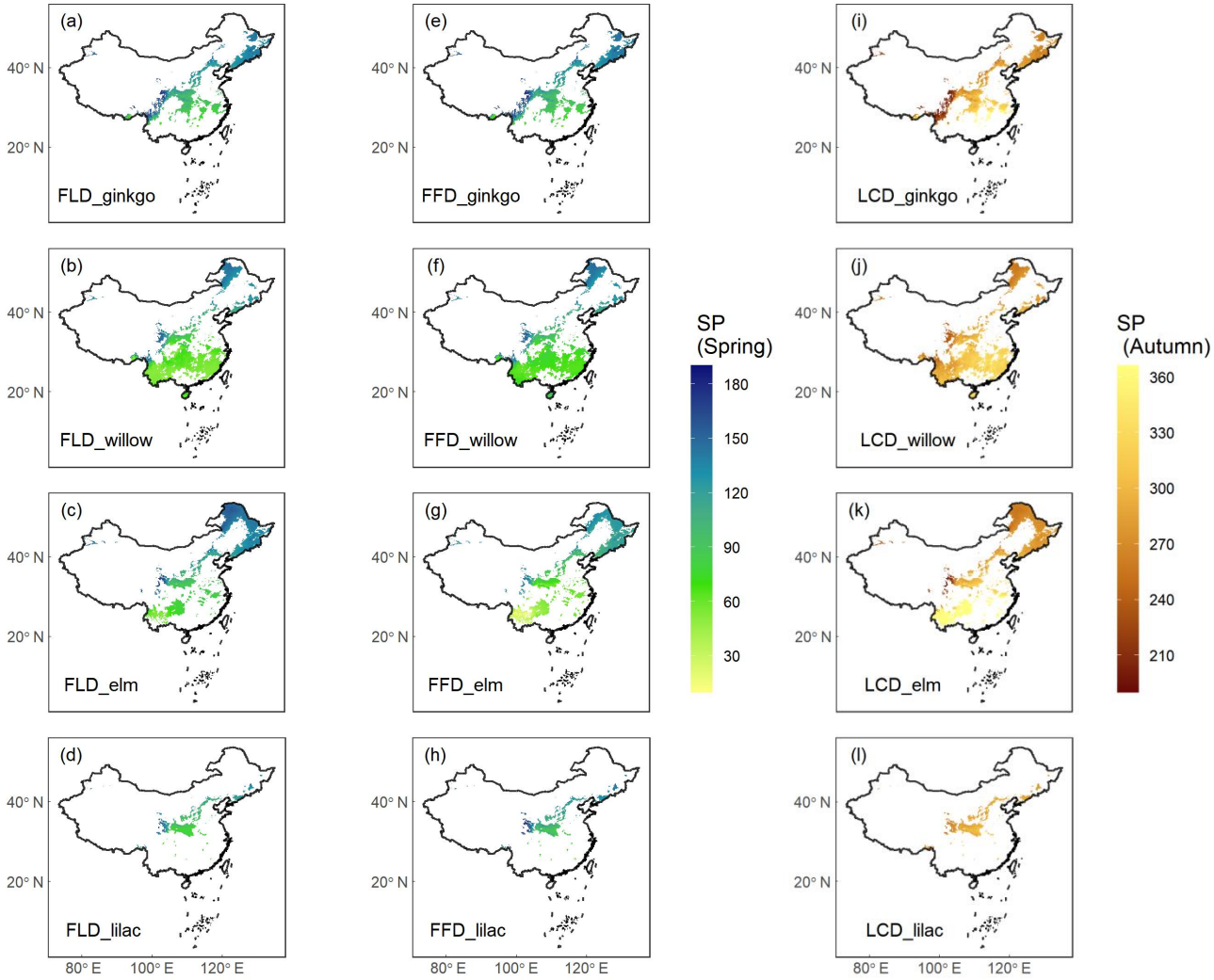

Figure 4: Species phenology (SP) maps of four typical woody species averaged from 1951 to 2020. Columns 1-2 show the spring phenophases (FLD and FFD), and Column 3 shows the autumn phenophase (LCD). Each row represents a species from ginkgo (*Ginkgo biloba*), willow (*Salix babylonica*), elm (*Ulmus pumila*), and lilac (*Syringa oblata*). The unit of phenology data is the Julian Day of year (DOY) from January 1st.

Table 2: The optimal phenology models and cross-validation results of 24 species. RMSE represents the root mean square error between the model simulated values and original values. R^2 represents goodness of fit of the optimal phenology model.

No.	Species	FLD			FFD			LCD		
		Optimal model	**RMSE**	R^2	**Optimal model**	**RMSE**	R^2	**Optimal model**	**RMSE**	R^2
1	*Ginkgo biloba*	TSC	7.30	0.669	TSC	7.53	0.553	DM	12.54	0.401
2	*Metasequoia glyptostroboides*	TSC	6.10	0.687	Unified	9.59	0.126	DM	9.99	0.295
3	*Magnolia denudata*	UniChill	6.47	0.781	TSC	7.33	0.576	DM	9.31	0.284
4	*Salix babylonica*	TSC	8.97	0.854	TSC	9.40	0.787	MR	18.23	0.380
5	*Populus × canadensis*	UniChill	5.94	0.808	UniChill	6.14	0.728	MR	9.45	0.139
6	*Robinia pseudoacacia*	TSC	5.47	0.863	TSC	6.18	0.785	DM	11.74	0.297
7	*Albizia julibrissin*	UniChill	7.48	0.500	Unified	8.23	0.376	MR	9.18	0.567
8	*Cercis chinensis*	TSC	7.90	0.723	UniChill	7.39	0.751	DM	9.09	0.175
9	*Prunus armeniaca*	TSC	6.05	0.865	UniChill	4.78	0.929	MR	14.52	0.191
10	*Ulmus pumila*	UniChill	5.09	0.901	UniChill	8.38	0.862	DM	11.16	0.654
11	*Morus alba*	TSC	6.70	0.905	UniChill	7.99	0.860	DM	9.04	0.175
12	*Broussonetia papyrifera*	UniChill	7.60	0.804	TSC	6.18	0.821	DM	9.97	0.615
13	*Quercus acutissima*	UniChill	6.73	0.931	UniChill	5.12	0.950	MR	14.35	0.765
14	*Pterocarya stenoptera*	UniChill	7.52	0.804	UniChill	7.89	0.710	MR	11.57	0.415
15	*Juglans regia*	TSC	6.04	0.739	UniChill	8.54	0.595	DM	8.41	0.141
16	*Betula platyphylla*	UniChill	3.80	0.915	UniChill	3.70	0.906	DM	8.27	0.655
17	*Acer pictum* subsp. *mono*	TSC	2.29	0.894	TSC	3.78	0.814	DM	4.71	0.670
18	*Ailanthus altissima*	UniChill	5.22	0.867	UniChill	8.34	0.664	DM	10.39	0.066
19	*Melia azedarach*	TSC	6.81	0.828	TSC	6.70	0.851	MR	10.19	0.135
20	*Firmiana simplex*	UniChill	6.02	0.694	Unified	8.10	0.314	DM	12.30	0.190
21	*Hibiscus syriacus*	TSC	9.66	0.666	Unified	13.38	0.331	DM	12.76	0.464
22	*Fraxinus chinensis*	TSC	6.25	0.852	Unified	12.35	0.319	MR	9.76	0.533
23	*Syringa oblata*	UniChill	7.01	0.864	UniChill	5.11	0.920	MR	12.36	0.475

24	*Paulownia fortunei*	UniChill	4.63	0.762	UniChill	7.02	0.693	MR	10.01	0.250

The effectiveness of the simulated SP maps was evaluated by cross-validation on the optimal phenology models (Table 2). The results showed that spring phenology yielded significantly more accurate simulations than autumn phenology (Fig. 5). Quantitatively, the RMSE for the optimal model of FLD (6.38 days) and FFD (7.46 days) in spring were significantly smaller than that of LCD (10.80 days) in autumn. Correspondingly, the R^2 for spring FLD (0.799) and FFD (0.676) was significantly higher compared to autumn LCD (0.372). When comparing the simulation effects of FLD and FFD in spring, no significant difference was observed. Among the optimal spring phenology models, the FFD simulations derived from the UniChill and TSC models demonstrated significantly better performance than those from the Unified model. Conversely, for autumn phenology, the simulations effects LCD were comparable between the MR and TP models.

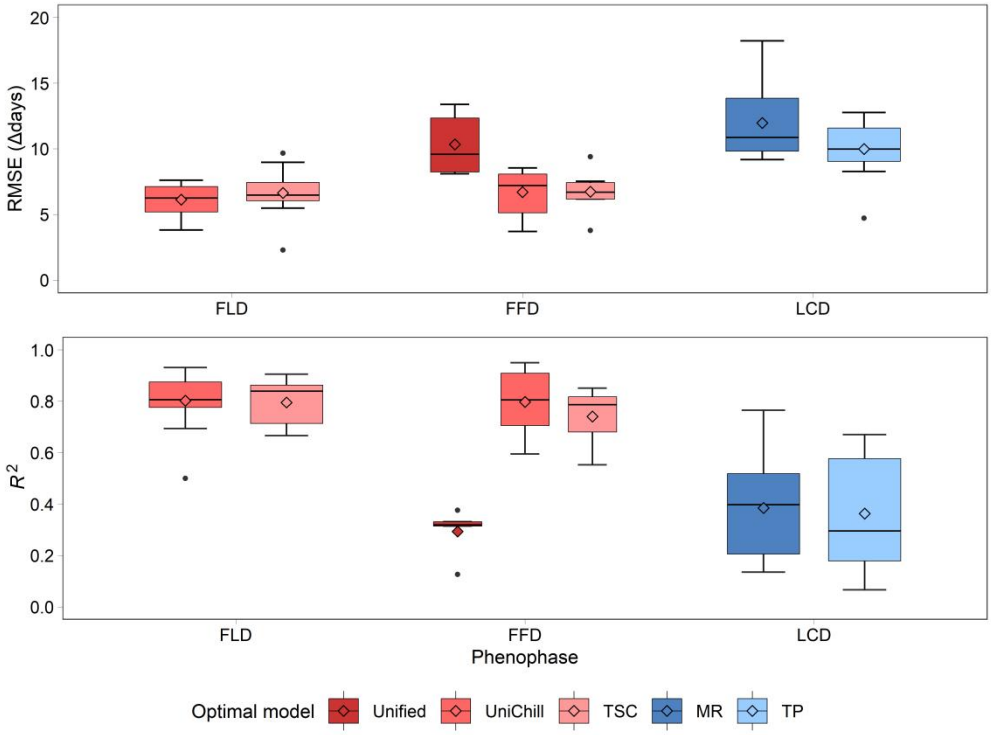

Figure 5: The RMSE (a) and R^2 (b) of cross-validation on the optimal phenology models for 24 woody species. Each model is represented by a different color, with warm colors for three spring phenology models (Unified, UniChill, TSC), and cool colors for two autumn phenology models (MR, TP). The model with the smallest RMSE was selected as the optimal model for each species. The horizontal line represents the median value, the diamond mark represents the mean value, and the dot mark represents the outlier in the boxplot.

3.2 Aggregation of ground phenology maps

The results of GP maps generated by four distinct aggregation methods (mean, pct50, pct20\80, pct10\90) exhibited similar spatial patterns (Fig. 6). These maps demonstrate a consistent pattern of phenological variation in relation to both latitude and altitude. Specifically, with increasing latitude or altitude, spring GP (FLD and FFD) occurred progressively later, while autumn GP (LCD) occurred earlier. When comparing the various aggregation methods, the GP maps aggregated by the mean and pct50 methods showed a high degree of consistency, with r being 0.992. In contrast, the GP maps aggregated by the pct20\80 and pct10\90 methods exhibited slightly more spatial variability and were less correlated with the former methods, with r being 0.968 and 0.949, respectively. The remarkable consistency between the maps aggregated through mean and pct50 methods suggests that both the weighted mean and weighted quantile approaches are robust and reliable for the aggregation of GP.

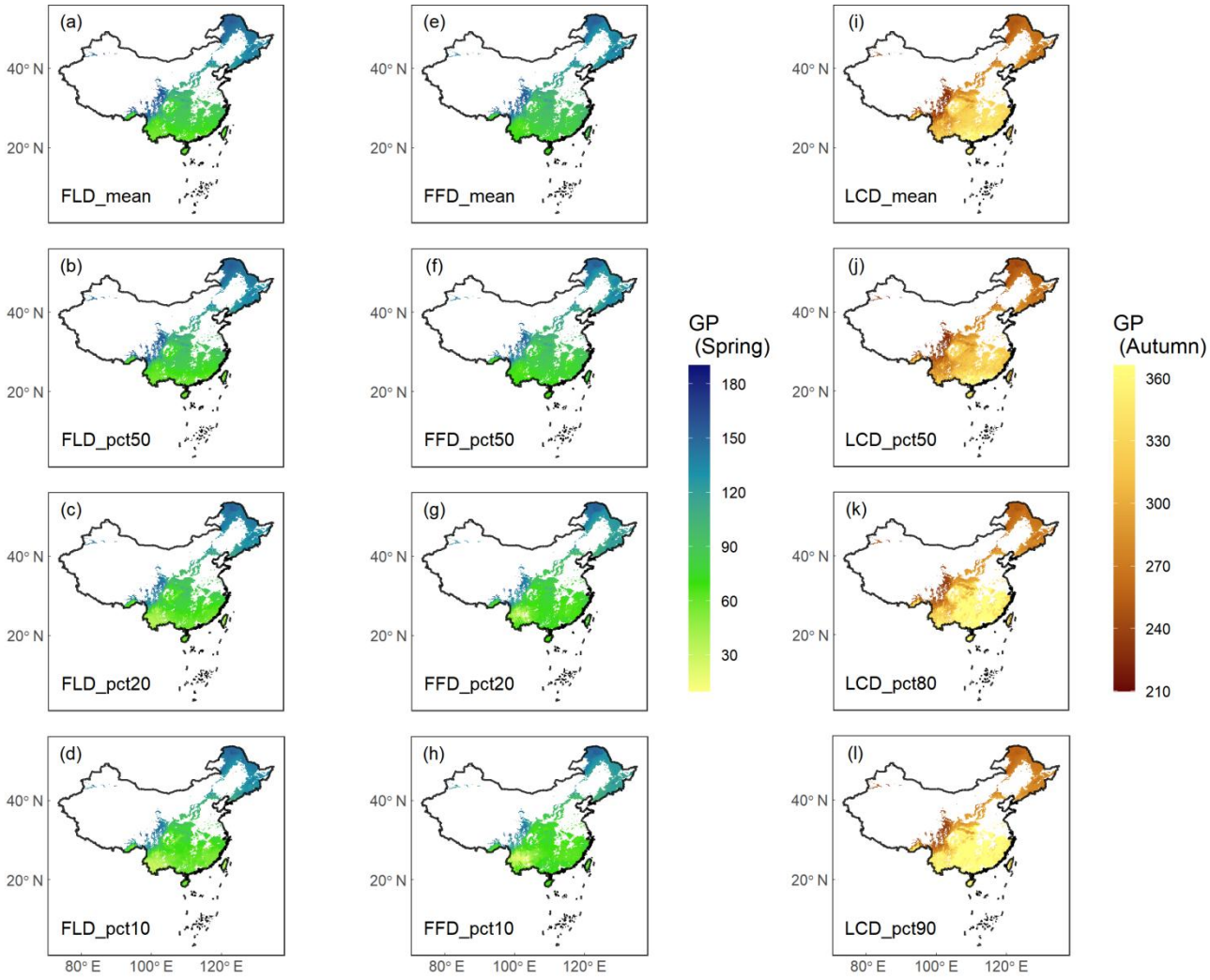

Figure 6: Ground phenology (GP) maps of four aggregation methods averaged from 1951 to 2020. Columns 1-2 show the spring phenophases (FLD and FFD), and Column 3 shows the autumn phenophase (LCD). Each row represents an aggregation method from weighted average (mean), weighted median (pct50), weighted 20% or 80% percentile (pct20\80), and weighted 10% or 90% percentile (pct10\90). The unit of GP is the Julian Day of year (DOY) from January 1st.

We have introduced two types of QA maps to assess the reliability of the aggregated GP maps (Fig. S1). The first QA map represents the total distribution probability of all species considered in the aggregation process, while the second QA map indicates the total number of species that have a distribution probability exceeding 0.1. In these QA maps, higher values correlate with a greater total number or higher cumulative probability of species within the aggregation, which signifies a higher reliability of GP maps for those particular areas. Notably, the most dependable GP aggregation results are distributed

around the 30° N latitude within China. In this region, the total number of species contributing to FLD and FFD is about 15, whereas for LCD, the number is around 6. However, it should be noted that the QA maps also identify areas where the GP aggregation may be less dependable. Specifically, in regions where the total number of species is fewer than 5 or the total probability is below 1, the reliability of the aggregated GP results may be compromised.

3.3 Data quality and usability

Our comparative analysis between GP and LSP focused on the FLD and SOS in spring, as well as the LCD and EOS in autumn across two periods (1981-2014 and 2013-2020). The results revealed that GP and two LSP products exhibited congruent spatial patterns in central and northern China, while discrepancies were more pronounced in southern China (Fig. 7), particularly regarding LCD and EOS in autumn (Fig. 7e-h). This is likely due to the prevalence of deciduous forests in central and northern China (Fig. 1). In contrast, southern China is characterized by a higher presence of evergreen and mixed forests. The GP maps in this study were derived from the phenological data of 24 deciduous woody plants species, which are well-represented in deciduous forests but less so in evergreen or mixed forests. Moreover, LSP metrics obtained from remote sensing data are generally more error-prone in evergreen and mixed forests due to the lack of obvious seasonal change and frequent cloud cover in these regions (Liu et al., 2016b). Consequently, the correlation between GP and LSP in evergreen or mixed forests was found to be relatively weak (Fig. S2), with the highest r being 0.44 in spring and 0.54 in autumn. and the lowest RMSE being 28.5 days in spring and 38.5 days in autumn (Table S2). In deciduous forests, however, the alignment between GP and LSP was substantially stronger, with the highest r being 0.95 in spring and 0.88 in autumn, and the lowest RMSE being 8.8 days in spring and 15.1 days in autumn, respectively.

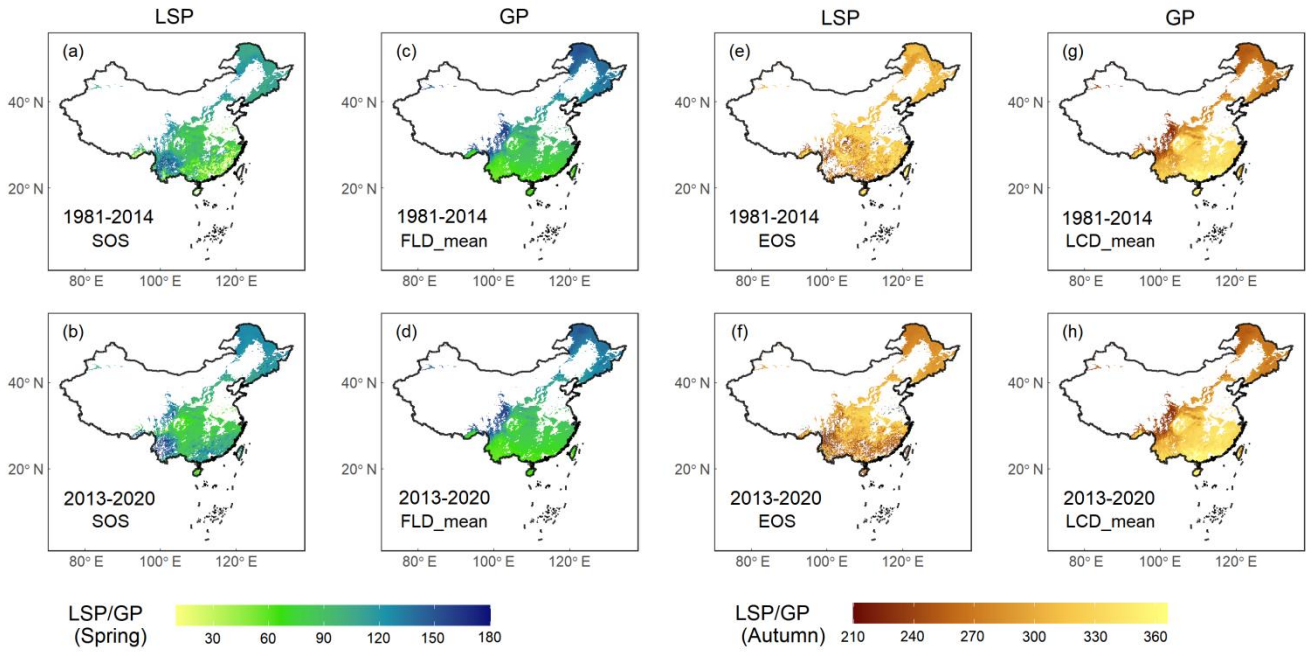

Figure 7: Comparison of GP maps in this study and two LSP products (VIPPHEN and VNP22C2) extracted from remote sensing in previous studies, which was made between FLD and SOS in spring and LCD and EOS in autumn. Row 1 shows the comparison between VIPPHEN product and GP map averaged in 1981-2014, and Row 2 shows the comparison between VNP22C2 product and GP map averaged in 2013-2020. (a-b) SOS from two LSP products; (c-d) FLD aggregated by mean method; (e-f) EOS from two LSP products; (g-h) LCD aggregated by mean method. The unit of GP or LSP is the Julian Day of year (DOY) from January 1st.

To further assess the data quality, we scrutinized the congruence between GP and LSP specifically within deciduous forests. The analysis indicated that GP and LSP exhibit a robust consistency for both VIPPHEN and VNP22C2 products, characterized by strong correlations, minor differences, and solid linear relationships (Fig. 8). The LSP derived from the VIPPHEN product demonstrated superior consistency with our study's GP compared to the VNP22C2 product's LSP. Furthermore, for both LSP products, the consistency between GP and LSP was significantly better in spring (Fig. 8e, g) than in autumn (Fig. 8f, h). When evaluating the influence of different aggregation methods on the GP and LSP correlation, no significant difference was observed in *r* among the methods (Fig. 8a, b). The consistency, as measured by *r*, was comparable across all methods, with values ranging from 0.76-0.78 in spring and 0.49-0.53 in autumn for the VIPPHEN product. For the VNP22C2 product, *r* values ranging from 0.90-0.91 in spring and 0.79-0.84 in autumn. Contrastingly,, the RMSE between GP and LSP varied notably across the different methods (Fig. 8c, d), which is largely attributable to the disparities in the average GP values generated by each method. The most effective aggregation methods, which yielded the smallest RMSE,

were pct10 (20.8 days) in spring and pct90 (32.9 days) in autumn for the VIPPHEN product. For the VNP22C2 product, pct20 (8.8 days) in spring and pct90 (15.1 days) in autumn were identified as the best methods.

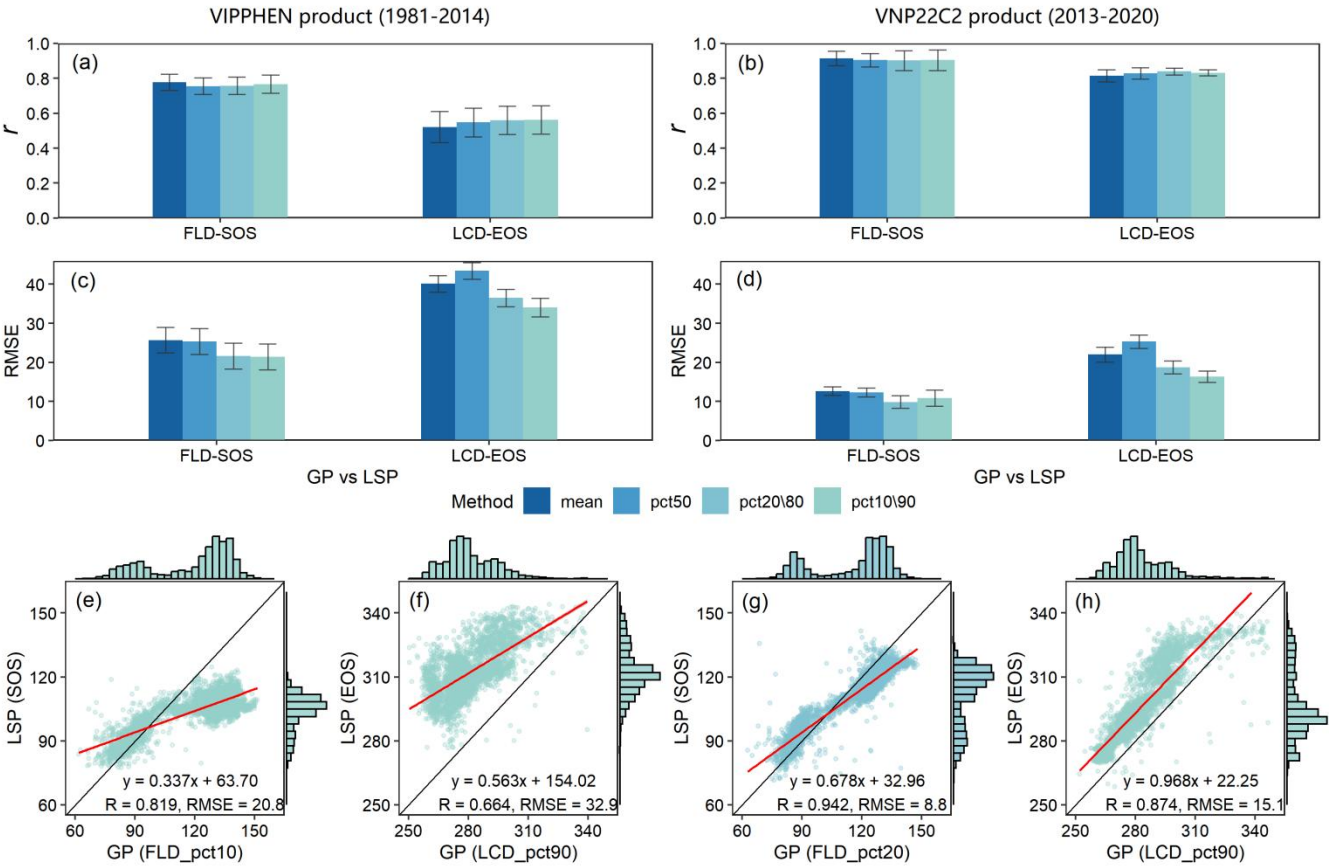

Figure 8: Comparison results of GP maps and two LSP products (VIPPHEN and VNP22C2) in deciduous forests, which was made between FLD and SOS in spring and LCD and EOS in autumn within the time range 1981-2014 and 2013-2020. (a-b) *r* between LSP and GP under four aggregating methods; (c-d) RMSE between LSP and GP under four aggregating methods; (e-h) Linear relationship between between LSP and GP under the best aggregating method. Each aggregating method is represented by a different color. The best aggregating method was determined by minimizing the RMSE between GP and LSP. The error bar in the bar plot represents the multi-year standard deviation. The red line in the scatter plot represents the linear regression line between GP and LSP, and all regression results were extremely significant ($p<0.001$).

The findings of this study highlight that the most accurate reflection of GP in comparison to LSP from remote sensing data occurs with the use of the 10th or 20th percentile for spring phenology and the 90th percentile for autumn phenology. This suggests that the onset of spring as detected by remote sensing aligns more closely with the FLD of the earliest emerging plant species (the first 10%-20%) on the ground. Conversely, the signal of vegetative dormancy in autumn from

remote sensing is in greater concordancet with the LCD of the last senescent plant species (the last 10%). Theseinsights are significant because they reveal a discernible link between GP and LSP, despite inherent differences in how these two types of phenology are measured. The consistency between early spring and late autumn events in GP and LSP underscores the potential for integrating these two phenological data sources to enhance our understanding of ecosystem dynamics and the effects of climate change on vegetative cycles.

The dataset represents a robust compilation of species and ground phenology simulations for forests of China over the past 70 years, distinguishing itself as an independent phenological data source derived from ground observations through modeling and aggregation. When applying this data, several factors must be considered::

(1) For SP maps, the accuracy is contingent upon the RMSE and R^2 resulting from cross-validation against the optimal phenology model for each species (Table 2). Additionally, the spatial reliability of phenology data is influenced by the density of observational sites per species (Table 1). For instance, while the FLD of *Betula platyphylla*'s exhibits high overall accuracy (RMSE = 3.80 and R^2 = 0.915), the accuracy may be compromised locally in areas with fewer observation sites (n = 13). Across the 24 species studied, SP maps consistently aligned with the in-situ observations, with an average error of 6.4 days for FLD, 7.5 days for FFD, and 10.8 days for LCD. These errors are comparable or lower than those reported in phenological studies from other regions. For example, simulation error of spring FLD and FFD was 7-9 days in central Europe (Basler, 2016) and was 12.3-12.7 days in the United States (Izquierdo-Verdiguier et al., 2018), while the simulation error of autumn LCD was 10.3-13.0 days in France (Delpierre et al., 2009) and 5.9-22.8 days in the United States (Jeong and Medvigy, 2014). Consequently,, compared with other studies on the regional scale, the SP maps of China in this study were found to have relatively high accuracy.

(2) For GP maps, data reliability can be assessed using QA maps, which reflect the total number or probability of species. Additionally, reliability can be evaluated by comparing GP maps with other LSP products, with a high degree of consistency indicating strong reliability. However, it is crucial to note that GP data primarily represent phenological estimates for deciduous forest components, resulting in higher reliability within deciduous forests and lower within evergreen or mixed forests. In this study, GP maps for forests in China demonstrated strong consistency with existing LSP products, especially within deciduous forests. The correlation coefficients of FLD and LCD were 0.91 and 0.84, respectively. Furthermore, the discrepancies between GP and LSP for FLD and LCD were relatively minor in deciduous forests, at 8.8 days and 15.1 days, respectively. Previous studies have reported lower consistency between LSP and single species phenology, with correlations ranging from 0.50 to 0.51 in the United States (Peng et al., 2017) and Germany (Kowalski et al., 2020), and discrepancies spanning 12 to 14.5 days in the United States (Peng et al., 2017) and Canada (Delbart et al., 2015). On the other hand, research comparing GP aggregates (average or quantile values) of multiple species has yielded better correlation coefficients, ranging from 0.61 to 0.71 in Europe (Rodriguez-Galiano et al., 2015; Tian et al., 2021), and 0.54 to 0.57 for the 30th percentile GP in China (Wu et al., 2016). These studies reported discrepancies between GP and LSP of 10.3-12.4 days in China (Wu et al., 2016), 13.9 days in Europe, and around 12.3 days in the United States (Ye et al., 2022), which are greater than the FLD discrepancies but less than those for LCD found in our study. While the

aggregated GP data derived from species-level phenology data in this study are generally reliable, it's important to recognize that limitations still exist in the available species-specific data, particularly when applied to evergreen or mixed forest regions..

(3) For phenology maps in different seasons, the phenology data exhibit significantly higher reliability for spring events compared to those in autumn. The underlying reason is that the biological processes underlying autumn phenology is more complex than those of spring (Menzel, 2002). Moreover, the mechanistic drivers of autumn phenology are intricate, which poses an additional challenge (Gill et al., 2015; Wu et al., 2018). For example, temperature has large effects on the autumn phenology than the spring phenology (Fu et al., 2018). In addition to temperature, other environmental factors such as precipitation (An et al., 2020), photoperiod (Lang et al., 2019), solar radiation (Wu et al., 2021b), spring phenology (Liu et al., 2016a), and growing-season productivity (Zani et al., 2020) also play significant roles in shaping autumn phenology. Given the multiplicity and complexity of these driving mechanisms, modeling autumn phenology becomes a more daunting task (Melaas et al., 2016). As a result, SP and GP maps for autumn manifest lower model performance and data quality relative to their spring counterparts.

4 Data availability

The annual SP and GP maps over China can be accessed at https://doi.org/10.57760/sciencedb.07995 (Zhu et al., 2023). This dataset is licensed under a CC-BY 4.0 license. The spatial reference system of the dataset is EPSG:4326(WGS84).

5 Conclusions

Leveraging historical observations from the CPON, this study introduces a novel, long-term gridded phenology dataset that includes SP maps for 24 woody plants species and GP maps of forests over China, covering the period from 1951 ot 2020. The dataset features a spatial resolution of 0.1° and a temporal resolution of 1 day. The SP maps were produced using a model-based upscaling method to extend the phenology data from in-situ observations to a regional scale across China. The GP maps were generated by employing weighted average and quantile methods to aggregate phenology data from the species to community and landscape levels. Quality assessments of the dataset indicate an average error for SP maps of 6.9 days in spring and 10.8 days in autumn. The smallest discrepancies between the GP maps and existing LSP products is 8.8 days for spring and 15.1 days for autumn. Compared to the previous studies (Basler, 2016; Delpierre et al., 2009; Izquierdo-Verdiguier et al., 2018; Jeong and Medvigy, 2014; Tian et al., 2021; Wu et al., 2016; Ye et al., 2022), the SP maps from this research exhibit comparable or smaller simulation errors, and the GP maps show strong concordance with other LSP products, underscoring the dataset's high accuracy and reliability. As the inaugural phenological map set for China, this dataset provides an invaluable tool for discerning the spatial patterns of plant phenology along the geographic gradient (e.g., longitude, latitude, and altitude). It also enables the examination of temporal trends (e.g., interannual, decadal, and secular)

in plant phenology throughout China. Moreover, the dataset offers critical support for research on the impacts of global change, aids in terrestrial ecosystem modeling, and contributes to natural resource management strategies.

Author contribution

QG and JD designed the study and planned the modeling. HW developed the model code. WL and YH performed the simulations. MZ processed the modeling data, performed the computations and drafted the manuscript. JD and JA critically revised the manuscript. All authors discussed and contributed to the modeling and manuscript.

Competing interests

The authors declare that they have no conflict of interest.

Acknowledgements

This study was jointly supported by National Key Research and Development Program of China (2018YFA0606102), National Natural Science Foundation of China (42271062), and Strategic Priority Research Program (A) of Chinese Academy of Sciences (XDA19020303; XDA26010202). Phenology data was provided by CPON. Temperature data was provided by Copernicus Climate Change Service (C3S).

References

An, S., Chen, X., Zhang, X., Lang, W., Ren, S., and Xu, L.: Precipitation and minimum temperature are primary climatic controls of alpine grassland autumn phenology on the Qinghai-Tibet Plateau, Remote Sens., 12, 431, https://doi.org/10.3390/rs12030431, 2020.

Aono, Y. and Kazui, K.: Phenological data series of cherry tree flowering in Kyoto, Japan, and its application to reconstruction of springtime temperatures since the 9th century, Int. J. Climatol., 28, 905–914, https://doi.org/10.1002/joc.1594, 2008.

Ault, T. R., Schwartz, M. D., Zurita-Milla, R., Weltzin, J. F., and Betancourt, J. L.: Trends and natural variability of spring onset in the coterminous United States as evaluated by a new gridded dataset of spring indices, J. Clim., 28, 8363–8378, https://doi.org/10.1175/jcli-d-14-00736.1, 2015.

Basler, D.: Evaluating phenological models for the prediction of leaf-out dates in six temperate tree species across central Europe, Agric. For. Meteorol., 217, 10–21, https://doi.org/10.1016/j.agrformet.2015.11.007, 2016.

Bolton, D. K., Gray, J. M., Melaas, E. K., Moon, M., Eklundh, L., and Friedl, M. A.: Continental-scale land surface phenology from harmonized Landsat 8 and Sentinel-2 imagery, Remote Sens. Environ., 240, 111685, https://doi.org/10.1016/j.rse.2020.111685, 2020.

Brown, J. H.: On the Relationship between Abundance and Distribution of Species, Am. Nat., 124, 255–279, https://doi.org/10.1086/284267, 1984.

Brun, P., Zimmermann, N., Hari, C., Pellissier, L., and Karger, D.: CHELSA-BIOCLIM+ A novel set of global climate-related predictors at kilometre-resolution, EnviDat [data set], 10, 2022a.

Brun, P., Zimmermann, N. E., Hari, C., Pellissier, L., and Karger, D. N.: Global climate-related predictors at kilometer resolution for the past and future, Earth Syst. Sci. Data, 14, 5573–5603, https://doi.org/10.5194/essd-14-5573-2022, 2022b.

Cai, H., Lyu, L., Shrestha, N., Tang, Z., Su, X., Xu, X., Dimitrov, D., and Wang, Z.: Geographical patterns in phylogenetic diversity of Chinese woody plants and its application for conservation planning, Divers. Distrib., 27, 179–194, https://doi.org/10.1111/ddi.13180, 2021.

Chuine, I.: A unified model for budburst of trees, J. Theor. Biol., 207, 337–347, https://doi.org/10.1006/jtbi.2000.2178, 2000.

Chuine, I., Cour, P., and Rousseau, D.: Fitting models predicting dates of flowering of temperate-zone trees using simulated annealing, Plant Cell Environ., 21, 455–466, https://doi.org/10.1046/j.1365-3040.1998.00299.x, 1998.

Chuine, I., Cambon, G., and Comtois, P.: Scaling phenology from the local to the regional level: advances from species-specific phenological models, Global Change Biol., 6, 943–952, https://doi.org/10.1046/j.1365-2486.2000.00368.x, 2000.

Cleland, E. E., Chuine, I., Menzel, A., Mooney, H. A., and Schwartz, M. D.: Shifting plant phenology in response to global change, Trends Ecol. Evol., 22, 357–365, https://doi.org/10.1016/j.tree.2007.04.003, 2007.

Dai, J., Wang, H., and Ge, Q.: Multiple phenological responses to climate change among 42 plant species in Xi'an, China, Int. J. Biometeorol., 57, 749–758, https://doi.org/10.1007/s00484-012-0602-2, 2013.

Dai, J., Wang, H., and Ge, Q.: Characteristics of spring phenological changes in China over the past 50 years, Adv. Meteorol., 2014, 1–8, https://doi.org/10.1155/2014/843568, 2014.

Delbart, N., Beaubien, E., Kergoat, L., and Le Toan, T.: Comparing land surface phenology with leafing and flowering observations from the PlantWatch citizen network, Remote Sens. Environ., 160, 273–280, https://doi.org/10.1016/j.rse.2015.01.012, 2015.

Delpierre, N., Dufrêne, E., Soudani, K., Ulrich, E., Cecchini, S., Boé, J., and François, C.: Modelling interannual and spatial variability of leaf senescence for three deciduous tree species in France, Agric. For. Meteorol., 149, 938–948, https://doi.org/10.1016/j.agrformet.2008.11.014, 2009.

Didan, K. and Barreto, A.: NASA MEaSUREs Vegetation Index and Phenology (VIP) Phenology NDVI Yearly Global 0.05Deg CMG, NASA EOSDIS Land Processes DAAC, accessed on 2022-08-11, https://doi.org/10.5067/MEaSUREs/VIP/VIPPHEN_NDVI.004, 2016.

Dixon, D. J., Callow, J. N., Duncan, J. M., Setterfield, S. A., and Pauli, N.: Satellite prediction of forest flowering phenology, Remote Sens. Environ., 255, 112197, https://doi.org/10.1016/j.rse.2020.112197, 2021.

Donnelly, A., Yu, R., Jones, K., Belitz, M., Li, B., Duffy, K., Zhang, X., Wang, J., Seyednasrollah, B., Gerst, K. L., and others: Exploring discrepancies between in situ phenology and remotely derived phenometrics at NEON sites, Ecosphere, 13, e3912, https://doi.org/10.1002/ecs2.3912, 2022.

Dronova, I. and Taddeo, S.: Remote sensing of phenology: Towards the comprehensive indicators of plant community dynamics from species to regional scales, J. Ecol., 110, 1460–1484, https://doi.org/10.1111/1365-2745.13897, 2022.

Estrella, N. and Menzel, A.: Responses of leaf colouring in four deciduous tree species to climate and weather in Germany, Clim. Res., 32, 253–267, https://doi.org/10.3354/cr032253, 2006.

Fang, J., Wang, Z., and Tang, Z.: Atlas of woody plants in China: distribution and climate, Springer Science & Business Media, 2011.

Fielding, A. H. and Bell, J. F.: A review of methods for the assessment of prediction errors in conservation presence/absence models, Environ. Conserv., 24, 38–49, https://doi.org/10.1017/s0376892997000088, 1997.

Fisher, J. I., Mustard, J. F., and Vadeboncoeur, M. A.: Green leaf phenology at Landsat resolution: Scaling from the field to the satellite, Remote Sens. Environ., 100, 265–279, https://doi.org/10.1016/j.rse.2005.10.022, 2006.

Fitchett, J. M., Grab, S. W., and Thompson, D. I.: Plant phenology and climate change: Progress in methodological approaches and application, Prog. Phys. Geogr., 39, 460–482, https://doi.org/10.1177/0309133315578940, 2015.

Friedl, M. and Sulla-Menashe, D.: MODIS/Terra+Aqua Land Cover Type Yearly L3 Global 500m SIN Grid V061, NASA EOSDIS Land Processes DAAC, https://doi.org/10.5067/MODIS/MCD12Q1.061, 2022.

Fu, Y., Li, X., Zhou, X., Geng, X., Guo, Y., and Zhang, Y.: Progress in plant phenology modeling under global climate change, Sci. China Earth Sci., 63, 1237–1247, https://doi.org/10.1007/s11430-019-9622-2, 2020.

Fu, Y. H., Zhao, H., Piao, S., Peaucelle, M., Peng, S., Zhou, G., Ciais, P., Huang, M., Menzel, A., Peñuelas, J., and others: Declining global warming effects on the phenology of spring leaf unfolding, Nature, 526, 104–107, https://doi.org/10.1038/nature15402, 2015.

Fu, Y. H., Piao, S., Delpierre, N., Hao, F., Hänninen, H., Liu, Y., Sun, W., Janssens, I. A., and Campioli, M.: Larger temperature response of autumn leaf senescence than spring leaf-out phenology, Global Change Biol., 24, 2159–2168, https://doi.org/10.1111/gcb.14021, 2018.

GBIF: GBIF Occurrence Download, accessed on 2022-08-12, https://doi.org/10.15468/dl.7dwjev, 2022.

Ge, Q., Wang, H., and Dai, J.: Simulating changes in the leaf unfolding time of 20 plant species in China over the twenty-first century, Int. J. Biometeorol., 58, 473–484, https://doi.org/10.1007/s00484-013-0671-x, 2014.

Ge, Q., Wang, H., Rutishauser, T., and Dai, J.: Phenological response to climate change in China: a meta-analysis, Global Change Biol., 21, 265–274, https://doi.org/10.1111/gcb.12648, 2015.

Gill, A. L., Gallinat, A. S., Sanders-DeMott, R., Rigden, A. J., Short Gianotti, D. J., Mantooth, J. A., and Templer, P. H.: Changes in autumn senescence in northern hemisphere deciduous trees: a meta-analysis of autumn phenology studies, Ann Bot, 116, 875–888, https://doi.org/10.1093/aob/mcv055, 2015.

Hufkens, K., Basler, D., Milliman, T., Melaas, E. K., and Richardson, A. D.: An integrated phenology modelling framework in R, Methods Ecol. Evol., 9, 1276–1285, https://doi.org/10.1111/2041-210x.12970, 2018.

Izquierdo-Verdiguier, E., Zurita-Milla, R., Ault, T. R., and Schwartz, M. D.: Development and analysis of spring plant phenology products: 36 years of 1-km grids over the conterminous US, Agric. For. Meteorol., 262, 34–41, https://doi.org/10.1016/j.agrformet.2018.06.028, 2018.

Jeong, S.-J. and Medvigy, D.: Macroscale prediction of autumn leaf coloration throughout the continental United States, Global Ecol. Biogeogr., 23, 1245–1254, https://doi.org/10.1111/geb.12206, 2014.

Keenan, T. F., Gray, J., Friedl, M. A., Toomey, M., Bohrer, G., Hollinger, D. Y., Munger, J. W., O'Keefe, J., Schmid, H. P., Wing, I. S., and others: Net carbon uptake has increased through warming-induced changes in temperate forest phenology, Nat. Clim. Change, 4, 598–604, https://doi.org/10.1038/nclimate2253, 2014.

Kowalski, K., Senf, C., Hostert, P., and Pflugmacher, D.: Characterizing spring phenology of temperate broadleaf forests using Landsat and Sentinel-2 time series, Int. J. Appl. Earth Obs. Geoinf., 92, 102172, https://doi.org/10.1016/j.jag.2020.102172, 2020.

Lang, W., Chen, X., Qian, S., Liu, G., and Piao, S.: A new process-based model for predicting autumn phenology: how is leaf senescence controlled by photoperiod and temperature coupling?, Agric. For. Meteorol., 268, 124–135, https://doi.org/10.1016/j.agrformet.2019.01.006, 2019.

Li, X., Zhou, Y., Meng, L., Asrar, G. R., Lu, C., and Wu, Q.: A dataset of 30 m annual vegetation phenology indicators (1985–2015) in urban areas of the conterminous United States, Earth Syst. Sci. Data, 11, 881–894, https://doi.org/10.5194/essd-11-881-2019, 2019.

Liang, L., Schwartz, M. D., and Fei, S.: Validating satellite phenology through intensive ground observation and landscape scaling in a mixed seasonal forest, Remote Sens. Environ., 115, 143–157, https://doi.org/10.1016/j.rse.2010.08.013, 2011.

Lieth, H.: Purposes of a phenology book, in: Phenology and Seasonality Modeling, edited by: Lieth, H., Springer, Berlin, Heidelberg, 3–19, https://doi.org/10.1007/978-3-642-51863-8_1, 1974.

Liu, H., Gong, P., Wang, J., Clinton, N., Bai, Y., and Liang, S.: Annual dynamics of global land cover and its long-term changes from 1982 to 2015, Earth Syst. Sci. Data, 12, 1217–1243, https://doi.org/10.5194/essd-12-1217-2020, 2020.

Liu, Q., Fu, Y. H., Zhu, Z., Liu, Y., Liu, Z., Huang, M., Janssens, I. A., and Piao, S.: Delayed autumn phenology in the Northern Hemisphere is related to change in both climate and spring phenology, Global Change Biol., 22, 3702–3711, https://doi.org/10.1111/gcb.13311, 2016a.

Liu, Y., Wu, C., Peng, D., Xu, S., Gonsamo, A., Jassal, R. S., Arain, M. A., Lu, L., Fang, B., and Chen, J. M.: Improved modeling of land surface phenology using MODIS land surface reflectance and temperature at evergreen needleleaf forests of central North America, Remote Sens. Environ., 176, 152–162, https://doi.org/10.1016/j.rse.2016.01.021, 2016b.

Melaas, E. K., Sulla-Menashe, D., Gray, J. M., Black, T. A., Morin, T. H., Richardson, A. D., and Friedl, M. A.: Multisite analysis of land surface phenology in North American temperate and boreal deciduous forests from Landsat, Remote Sens. Environ., 186, 452–464, https://doi.org/10.1016/j.rse.2016.09.014, 2016.

Menzel, A.: Phenology: its importance to the global change community, Clim. Change, 54, 379, https://doi.org/10.1023/A:1016125215496, 2002.

Menzel, A., Yuan, Y., Matiu, M., Sparks, T., Scheifinger, H., Gehrig, R., and Estrella, N.: Climate change fingerprints in recent European plant phenology, Global Change Biol., 26, 2599–2612, https://doi.org/10.1111/gcb.15000, 2020.

Misra, G., Cawkwell, F., and Wingler, A.: Status of phenological research using Sentinel-2 data: A review, Remote Sens., 12, 2760, https://doi.org/10.3390/rs12172760, 2020.

Muñoz Sabater, J.: ERA5-Land hourly data from 1981 to present, Copernicus Climate Change Service (C3S) Climate Data Store (CDS), 2019.

Muñoz Sabater, J.: ERA5-Land hourly data from 1950 to 1980, Copernicus Climate Change Service (C3S) Climate Data Store (CDS), 2021.

Muñoz-Sabater, J., Dutra, E., Agustí-Panareda, A., Albergel, C., Arduini, G., Balsamo, G., Boussetta, S., Choulga, M., Harrigan, S., Hersbach, H., and others: ERA5-Land: A state-of-the-art global reanalysis dataset for land applications, Earth Syst. Sci. Data, 13, 4349–4383, https://doi.org/10.5194/essd-13-4349-2021, 2021.

Park, D. S., Newman, E. A., and Breckheimer, I. K.: Scale gaps in landscape phenology: challenges and opportunities, Trends Ecol. Evol., 36, 709–721, https://doi.org/10.1016/j.tree.2021.04.008, 2021.

Peng, D., Wu, C., Li, C., Zhang, X., Liu, Z., Ye, H., Luo, S., Liu, X., Hu, Y., and Fang, B.: Spring green-up phenology products derived from MODIS NDVI and EVI: Intercomparison, interpretation and validation using National Phenology Network and AmeriFlux observations, Ecol. Indic., 77, 323–336, https://doi.org/10.1016/j.ecolind.2017.02.024, 2017.

Phillips, S. J., Anderson, R. P., and Schapire, R. E.: Maximum entropy modeling of species geographic distributions, Ecol. Modell., 190, 231–259, https://doi.org/10.1016/j.ecolmodel.2005.03.026, 2006.

Piao, S., Liu, Q., Chen, A., Janssens, I. A., Fu, Y., Dai, J., Liu, L., Lian, X., Shen, M., and Zhu, X.: Plant phenology and global climate change: Current progresses and challenges, Glob Chang Biol, 25, 1922–1940, https://doi.org/10.1111/gcb.14619, 2019.

Polgar, C. A. and Primack, R. B.: Leaf-out phenology of temperate woody plants: from trees to ecosystems, New Phytol., 191, 926–941, https://doi.org/10.1111/j.1469-8137.2011.03803.x, 2011.

Pukelsheim, F.: The three sigma rule, Am. Stat., 48, 88–91, https://doi.org/10.2307/2684253, 1994.

Richardson, A. D., Keenan, T. F., Migliavacca, M., Ryu, Y., Sonnentag, O., and Toomey, M.: Climate change, phenology, and phenological control of vegetation feedbacks to the climate system, Agric. For. Meteorol., 169, 156–173, https://doi.org/10.1016/j.agrformet.2012.09.012, 2013.

Richardson, A. D., Hufkens, K., Milliman, T., Aubrecht, D. M., Chen, M., Gray, J. M., Johnston, M. R., Keenan, T. F., Klosterman, S. T., Kosmala, M., and others: Tracking vegetation phenology across diverse North American biomes using PhenoCam imagery, Sci. Data, 5, 1–24, https://doi.org/10.1038/sdata.2018.28, 2018.

Rodriguez-Galiano, V., Dash, J., and Atkinson, P. M.: Intercomparison of satellite sensor land surface phenology and ground phenology in Europe, Geophys. Res. Lett., 42, 2253–2260, https://doi.org/10.1002/2015gl063586, 2015.

Sagarin, R. D. and Gaines, S. D.: The 'abundant centre' distribution: to what extent is it a biogeographical rule?, Ecol. Lett., 5, 137–147, https://doi.org/10.1046/j.1461-0248.2002.00297.x, 2002.

Schwartz, M. D.: Phenology: an integrative environmental science, Springer, 2003.

Studer, S., Stöckli, R., Appenzeller, C., and Vidale, P. L.: A comparative study of satellite and ground-based phenology, Int. J. Biometeorol., 51, 405–414, https://doi.org/10.1007/s00484-006-0080-5, 2007.

Tang, J., Körner, C., Muraoka, H., Piao, S., Shen, M., Thackeray, S. J., and Yang, X.: Emerging opportunities and challenges in phenology: a review, Ecosphere, 7, e01436, https://doi.org/10.1002/ecs2.1436, 2016.

Tao, Z., Wang, H., Dai, J., Alatalo, J., and Ge, Q.: Modeling spatiotemporal variations in leaf coloring date of three tree species across China, Agric. For. Meteorol., 249, 310–318, https://doi.org/10.1016/j.agrformet.2017.10.034, 2018.

Templ, B., Koch, E., Bolmgren, K., Ungersböck, M., Paul, A., Scheifinger, H., Rutishauser, T., Busto, M., Chmielewski, F.-M., Hájková, L., and others: Pan European Phenological database (PEP725): a single point of access for European data, Int. J. Biometeorol., 62, 1109–1113, https://doi.org/10.1007/s00484-018-1512-8, 2018.

Tian, F., Cai, Z., Jin, H., Hufkens, K., Scheifinger, H., Tagesson, T., Smets, B., Van Hoolst, R., Bonte, K., Ivits, E., and others: Calibrating vegetation phenology from Sentinel-2 using eddy covariance, PhenoCam, and PEP725 networks across Europe, Remote Sens. Environ., 260, 112456, https://doi.org/10.1016/j.rse.2021.112456, 2021.

Wang, H., Dai, J., and Ge, Q.: The spatiotemporal characteristics of spring phenophase changes of Fraxinus chinensis in China from 1952 to 2007, Sci. China Earth Sci., 55, 991–1000, https://doi.org/10.1007/s11430-011-4349-0, 2012.

Wang, H., Wu, C., Ciais, P., Peñuelas, J., Dai, J., Fu, Y., and Ge, Q.: Overestimation of the effect of climatic warming on spring phenology due to misrepresentation of chilling, Nat. Commun., 11, 4945, https://doi.org/10.1038/s41467-020-18743-8, 2020.

Wu, C., Hou, X., Peng, D., Gonsamo, A., and Xu, S.: Land surface phenology of China's temperate ecosystems over 1999–2013: Spatial–temporal patterns, interaction effects, covariation with climate and implications for productivity, Agricultural and Forest Meteorology, 216, 177–187, https://doi.org/10.1016/j.agrformet.2015.10.015, 2016.

Wu, C., Wang, X., Wang, H., Ciais, P., Peñuelas, J., Myneni, R. B., Desai, A. R., Gough, C. M., Gonsamo, A., Black, A. T., and others: Contrasting responses of autumn-leaf senescence to daytime and night-time warming, Nat. Clim. Change, 8, 1092–1096, https://doi.org/10.1038/s41558-018-0346-z, 2018.

Wu, W., Sun, Y., Xiao, K., and Xin, Q.: Development of a global annual land surface phenology dataset for 1982–2018 from the AVHRR data by implementing multiple phenology retrieving methods, Int. J. Appl. Earth Obs. Geoinf., 103, 102487, https://doi.org/10.1016/j.jag.2021.102487, 2021a.

Wu, Z., Chen, S., De Boeck, H. J., Stenseth, N. C., Tang, J., Vitasse, Y., Wang, S., Zohner, C., and Fu, Y. H.: Atmospheric brightening counteracts warming-induced delays in autumn phenology of temperate trees in Europe, Global Ecol. Biogeogr., 30, 2477–2487, https://doi.org/10.1111/geb.13404, 2021b.

Ye, Y., Zhang, X., Shen, Y., Wang, J., Crimmins, T., and Scheifinger, H.: An optimal method for validating satellite-derived land surface phenology using in-situ observations from national phenology networks, ISPRS J. Photogramm. Remote Sens., 194, 74–90, https://doi.org/10.1016/j.isprsjprs.2022.09.018, 2022.

Zani, D., Crowther, T. W., Mo, L., Renner, S. S., and Zohner, C. M.: Increased growing-season productivity drives earlier autumn leaf senescence in temperate trees, Science, 370, 1066–1071, https://doi.org/10.1126/science.abd8911, 2020.

Zhang, X., Wang, J., Gao, F., Liu, Y., Schaaf, C., Friedl, M., Yu, Y., Jayavelu, S., Gray, J., Liu, L., and others: Exploration of scaling effects on coarse resolution land surface phenology, Remote Sens. Environ., 190, 318–330, https://doi.org/10.1016/j.rse.2017.01.001, 2017.

Zhang, X., Friedl, M., and Henebry, G.: VIIRS/NPP Land Cover Dynamics Yearly L3 Global 0.05 Deg CMG V001, NASA EOSDIS Land Processes DAAC, accessed on 2022-08-11, https://doi.org/10.5067/VIIRS/VNP22C2.001, 2020.

Zhu, M., Dai J.: Species phenology and ground phenology maps over China from 1951-2020, Science Data Bank [data set], https://doi.org/10.57760/sciencedb.07995. DOI:10.57760/sciencedb.07995, 2023.